Abdominal Radiology (2019) 44:1841–1849
https://doi.org/10.1007/s00261-019-01897-5

KIDNEYS, URETERS, BLADDER, RETROPERITONEUM

Usefulness of rapid kV-switching dual energy CT in renal tumor characterization

İlkay Çamlıdağ[1] · Mehmet Selim Nural[1] · Murat Danacı[1] · Ender Özden[2]

Published online: 14 January 2019

Abstract

Purpose To investigate whether iodine content can discriminate between benign or malignant renal tumors, malign tumor subtypes, low-grade and high-grade tumors on rapid kv-switching dual-energy CT (rsDECT).

Methods This prospective study enrolled 95 patients with renal tumors who underwent rsDECT for tumor characterization between 2016 and 2018. Attenuation on true and virtual unenhanced images, absolute enhancement and enhancement ratio and iodine content of each lesion on nephrographic phase iodine density images were measured. Histopathological diagnosis was obtained following either surgery or core biopsy.

Results Eighty-five tumors were renal cell carcinoma (RCC) (56 clear cell, 20 papillary, 9 chromophobe) and 10 were benign (6 angiomyolipoma,4 oncocytoma). 46 tumors were low-grade and 23 high-grade. There was significant difference between iodine content of clear cell and non-clear cell (papillary + chromophobe) RCC ($p < 0.001$). However, no significant iodine content differences were found between papillary and chromophobe RCC, benign and malignant tumors, low-grade and high-grade tumors. The best cut-off iodine content for differentiating clear cell from non-clear cell RCC was 3.2 mg/ml and clear cell from papillary RCC was 2.9 mg/ml with a high sensitivity and specificity. Also, significant difference was found between attenuation values of true and virtual unenhanced images ($p = 0.007$). Mean iodine content, absolute enhancement and enhancement ratio were highly correlated.

Conclusion rsDECT contributes to renal tumor characterization by showing higher iodine content in clear cell RCCs compared with non-clear cell RCCs.

Keywords Rapid kV-switching dual energy CT · Renal tumor · Iodine content

Introduction

Technical advances in abdominal cross-sectional imaging and its increased use for various indications have resulted in increased renal tumor detection and majority of these masses turned out to be renal cell carcinoma (RCC) [1]. More than 70% of the RCCs are comprised of clear cell subtype, 10-15% are papillary, 5% chromophobe and the rest are other rare subtypes. RCC subtype is the major prognostic factor and clear cell RCC has a poorer prognosis when compared to papillary and chromophobe subtypes [2, 3]. Therefore, imaging has a paramount role in characterizing the tumor as benign or malignant, differentiate the subtype if it is presumed to be malignant and to categorize high risk or low risk tumors that would have an impact on clinical decision and patient outcome. However, characterization is not always easy and straightforward when the mass is small and do not carry the diagnostic clues for specific renal tumors on conventional computed tomography (CT) or magnetic resonance imaging (MRI) like macroscopic fat presence for fat-rich angiomyolipoma (AML) [4], ice cream cone pattern for fat-poor AML [5], central scar or segmental enhancement inversion for oncocytoma [6, 7], and typical enhancement patterns. Moreover, even when present, these diagnostic clues are not specific enough for differentiating benign from malignant masses and subtype differentiation with the exception of macroscopic fat presence for fat-rich AML. For this reason, attempts have been made to be able to find a biomarker for more accurate renal tumor characterization.

✉ İlkay Çamlıdağ
ilkayozaydin@hotmail.com

[1] Department of Radiology, Ondokuz Mayıs University, Kurupelit, 55210 Samsun, Turkey

[2] Department of Urology, Ondokuz Mayıs University, Kurupelit, 55210 Samsun, Turkey

Dual-energy CT (DECT) technology has recently been introduced into clinical practice and provides material decomposition into its constituent elements by taking advantage of the change in attenuation of materials with different photon energy to provide additional quantitative and qualitative data which single energy CT can not provide. The high- and low-energy data are provided by either using two different X-ray tubes for simultaneous acquisition of the projection data (dual-source DECT) or a single X-ray tube which switches high- and low-energy output between alternating projections (rapid kv-switcing DECT) [8–10]. Although there are four other commercially available systems with different technologies, dual-source DECT and rapid kv-switching DECT (rsDECT) systems are more available clinically and provided more accurate results for iodine and monochromatic accuracy in a phantom study [11].

DECT has proved to be very useful and beneficial in genitourinary applications and especially in renal lesion characterisation by providing virtual unenhanced images obviating the need for true unenhanced images which is otherwise necessary for evaluation of enhancement within a lesion in a single energy acquisition [12–15]. Moreover, enhancement can be directly and more reliably depicted on iodine density images which map the iodine content of tissues either by visually or quantitatively [8]. Renal lesion pseudoenhancement which is defined as the artefactual increase in attenuation of a small or centrally located simple renal cyst due to beam-hardening effects could be reduced by virtual monochromatic images provided by DECT [9, 16, 17].

Recently, a few number of studies have been published regarding RCC carcinoma subtype differentiation based on lesion iodine content on DECT and they provided different iodine thresholds because of dual-energy system differences [18–20]. These studies mainly focused on clear cell-papillary RCC differentiation and only one of them also included the chromophobe type [18], but none of them included benign renal masses. Also, only one of these studies [20] was performed on a rsDECT platform. Therefore, their findings require validation. Hence, we aimed to assess whether quantitative iodine content of a renal tumor in the nephrographic phase could help RCC subtype differentiation, malignant tumor grading, and benign-malignant differentiation by rsDECT. The rationale for selecting nephrographic phase was because majority of renal tumors reach their enhancement peak in this phase.

Materials and methods

This was a prospective study and institutional review board approved the study. All included patients gave their informed consent prior to study.

Patient selection

One hundred and twenty patients with 120 incidentally detected renal tumors by ultrasound or other modalities in outsided hospitals who were referred for renal mass characterization were prospectively enrolled between May 2016 and September 2018. Patients whose histopathological examinations were obtained by either partial or radical nephrectomy, or core biyopsies on follow-up were eligible for the study. Patients with fat-rich angiomyolipoma (AML) on CT (2 patients) or histopathological diagnoses other than clear cell, papillary, chromophobe RCC, fat-poor AML and oncocytoma (4 patients) were excluded from the study. Of these patients, one had a papillary adenoma, one had a benign proteinaceous cyst, one had a plasmocytoma, and one had a tubulocystic renal cell carcinoma. Patients who were decided to have active surveillance (2 patients) or who had no further records of operation or biopsy in the hospital database after the CT examination (17 patients) were also excluded from the study due to the absence of final histopathological results. Finally, 95 patients with 95 tumors met the enrollment criteria between the mentioned dates.

Dual-energy CT protocol

CT examinations were performed on a rapid kV-switching dual-energy 64-detector MDCT scanner (Discovery CT750 HD scanner, General Electric Healthcare, Waukesha, WI, USA). As all the patients were referred with the clinical request of renal mass characterization, standard protocol of our institution for renal mass characterization consisting of unenhanced, nephrographic and excretory phase imaging were applied. Standard unenhanced images covering the whole kidneys were obtained using a conventional 120 kVp polychromatic beam multidetector CT technique (scan type, helical, detector coverage, 40 mm, slice thickness 5 mm, interval, 1.25 mm, pitch, 1.375:1, speed, 55, and gantry rotation time, 0.7 s). Intravenous contrast material was then administered (Iohexol: Omnipaque 350, General Electronic Healthcare, Princeton NJ, USA) using a standardized weight-based dose injected at 2.5–4.0 cc/s rate for a fixed 30-s injection interval, followed by a 25 cc normal saline bolus injected at the same rate as the contrast. Nephrographic phase CT images were acquired in dual-energy mode at 90 s after the contrast injection covering the upper abdomen(scan type, helical, detector coverage, 40 mm, slice thickness, 2.5 mm, interval, 1.25 mm, pitch, 0.984:1, speed, 39.37, and gantry rotation time, 0.7 s). Excretory phase images were acquired by conventional single energy CT protocol with identical parameters

to unenhanced CT except for the slice thickness which was 2.5 mm at 7 min after contrast injection again covering the whole kidneys. The conventional and dual-energy images were sent to dual-energy workstation for routine clinical evaluation and further analysis.

Image analysis

All analyses were performed on dual-energy workstation (the Gemstone Spectral Image (GSI) Viewer, ADW 2.0, General Electric Healthcare, Milwaukee, WI) by a board-certified radiologist with 4 years of experience in abdominal radiology during the reporting of each CT examination before sampling or surgery. Therefore, the radiologist was blinded to the final histopathological results of the masses. After largest lesion diameter was measured in millimeters, the mean lesion attenuation in Hounsfield units (HU) was measured on the unenhanced, virtual unenhanced, nephrographic phase and excretory phase images. Iodine content on material density images was calculated in mg/ml. For homogenous lesions, the slice where the lesion was largest and for heterogenous cystic-necrotic lesions, the slice which contained the largest area of the most avidly enhancing part of the tumor were chosen for analyses on nephrographic phase images. Regions of interest (ROIs) encompassed the lesion in homogenous lesions as much as possible whereas it included the most avidly enhancing part in cystic-necrotic lesions. ROIs were kept identical by copying the ROI drawn on monochromatic nephrographic phase image onto the virtual unenhanced and iodine density images at the same single slice in the reformat mode of GSI viewer. True unenhanced images obtained in conventional single energy mode were opened in standard reformat viewer of the AW server and attenuation measurements were performed on the same slice that dual-energy analyses were performed with the same ROI size. Absolute enhancement was calculated as the difference in mean HU between nephrographic phase and true unenhanced image. Enhancement ratio was calculated as absolute enhancement divided by the mean HU in true unenhanced image. CT dose index volume (CTDIvol) and dose length product (DLP) of each phase were recorded in mGy and mGy*cm.

Histopathological analysis

Patients with masses reported as probable renal cell carcinoma or indeterminate as benign or malignant on CT underwent either core biopsy (6 patients), laparoscopic partial (59 patients) or radical nephrectomy procedures (30 patients) and specimens were sent to pathology department for microscopic analysis.

A board-certified pathologist who was involved in genitourinary pathology reviewed all tumors based on hematoxylin and eosin preparation and immunohistochemical staining. Final diagnoses, tumor subtypes and grades were given in the pathological reports. Fuhrman grade I and and II tumors were assigned as low-grade tumors whereas grade III and IV tumors assigned to high-grade category.

Statistical analysis

Statistical analysis was carried out using SPSS 22.0 software package. Data were presented as means ± standard deviations (SD). Papillary and chromophobe renal cell carcinoma was separately categorized as non-clear cell RCC. Student t test was used for comparison between iodine contents of clear cell and non-clear cell RCC, benign and malignant tumors, low-grade and high-grade tumors. Paired t test was used to compare attenuation values on true and virtual unenhanced images. One-way ANOVA and post hoc Tukey test was used for multiple comparisons between each tumor subtype. Receiver operating characteristics (ROC) analysis was performed to evaluate the diagnostic performance of iodine content for differentiating clear cell from papillary and non-clear cell RCC. The optimum cut-off point was determined as the value that discriminated between these subtypes the best in terms of maximum sensitivity and specificity. Pearson correlation analysis was used to investigate the correlation between iodine content and absolute enhancement-enhancement ratio and true-virtual unenhanced attenuation values. Kruskall Wallis H test and one-way ANOVA and post hoc Tukey test was used to compare CTDIvol and DLP between different phases of the CT examination. The level of statistical significance was set as $p < 0.05$.

Results

Table 1 demonstrates patient and tumor characteristics. Sixty three patients were male and 32 patients were female. Mean patient age was 59 years (range 21–84). Mean tumor size was 48 mm (range 13–187). 85 tumors were malignant (56 clear cell, 20 papillary, 9 chromophobe RCC and 10 were benign (6 fat-poor AML, 4 oncocytoma). 46 patients had low-grade whereas 21 patients had high-grade tumors.

Mean iodine content, absolute enhancement and enhancement ratio of each tumor subtype is demonstrated in Table 2. There was significant difference between mean iodine content of clear cell (Fig. 1) and papillary RCC (Fig. 2): 4.5 ± 1.2 mg/ml versus 2 ± 0.7 mg/ml, ($p < 0.001$). There was also significant difference between mean iodine content of clear cell and non-clear cell RCC (papillary + chromophobe): 4.5 ± 1.2 mg/ml versus 2.2 ± 0.7 mg/ml, ($p < 0.001$). Mean iodine content of chromophobe RCC (Fig. 3) was 2.6 ± 0.7 mg/ml and significantly different from clear cell RCC. No significant difference was found

Table 1 Patient and tumor characteristics

Variable	Value
Patient age (median, range)	59 years (21–84)
Patient number	95
Male	63 (66%)
Female	32 (34%)
Tumor size (mean ± SD, range)	48 ± 3 mm (13–187)
Benign vs. malignant	
Benign	10 (10.5%)
Malignant	85 (89.5%)
Benign tumors	
AML	6 (6%)
Oncocytoma	4 (4%)
RCC subtypes	
Clear cell	56 (59%)
Papillary	20 (21%)
Chromophobe	9 (9%)
Fuhrman grade	
Low grade (grade I + II)	46 (67%)
High grade (grade III + IV)	23 (33%)

sd standard deviation, *RCC* carcinoma, *AML* angiomyolipoma

Table 2 Mean iodine content in nephrographic phase, absolute enhancement and enhancement ratio according to renal tumor subtypes

	Mean iodine content (mg/ml)	Absolute enhancement (HU)	Enhancement ratio
Clear cell RCC	4.5 ± 1.2^{a}	91.5 ± 29.5^{a}	2.7 ± 1.2^{a}
Papillary RCC	2 ± 0.7^{b}	36.8 ± 14.8^{bc}	1.1 ± 0.6^{b}
Chromophobe RCC	2.6 ± 0.7^{b}	49.6 ± 16.6^{bc}	1.6 ± 0.6^{b}
Fat-poor AML	3.3 ± 1^{ab}	59.7 ± 15.4^{bc}	1.5 ± 0.6^{ab}
Oncocytoma	3.4 ± 1.7^{ab}	64.8 ± 44.1^{abc}	2 ± 1.2^{ab}

Means in the same column without a common superscript letter differ ($p < 0.05$) as analyzed by one-way ANOVA

between the iodine content of papillary and chromophobe RCC ($p = 0.64$). Mean iodine content of low-grade and high-grade tumors were 4.2 ± 2.2 mg/ml and 3.8 ± 1.5 mg/ml, mean iodine content of malignant and benign tumors (Figs. 4, 5) were 3.7 ± 1.5 mg/ml and 3.4 ± 1.2 mg/ml, respectively. However, no significant difference was found between the iodine content of low-grade and high-grade tumors, malignant and benign tumors ($p > 0.05$). The best cut-off iodine content for differentiating clear cell from papillary RCC was 2.9 mg/ml and clear cell from non-clear cell RCC was 3.2 mg/ml in nephrographic phase imaging. The ROC curve analyses results can be found in Table 3.

Mean attenuation of tumors on true and virtual unenhanced images were 38.7 ± 8.5 HU and 37.2 ± 8.6 HU respectively. There was significant difference between attenuation values on true and virtual unenhanced images ($p = 0.007$) and attenuation values were very well correlated ($r = 0.84$). There was a very good correlation between absolute enhancement, enhancement ratio and iodine content. Scatter plots of Pearson correlation can be found in Fig. 5.

Mean CTDIvol of the unenhanced, nephrographic phase and excretory phase was $8{,}65 \pm 4.78$ mGy, 18.34 ± 6.54 mGy and 15.27 ± 4.42 mGy respectively. There was no significant difference between CTDIvol values of the nephrographic and excretory phases ($p = 0.631$); however it was significantly different between unenhanced-nephrographic phase ($p < 0.001$) and unenhanced-excretory phase ($p = 0.001$). Mean DLP of the unenhanced, nephrographic phase and excretory phase was 318.52 ± 150.34, 754.15 ± 236.09 and 511.59 ± 165.08 mGy*cm respectively. There were significant differences between DLPs of different phases in pairwise comparisons ($p < 0.001$). Mean total DLP was calculated as 1568.86 ± 407.14 mGy*cm.

Discussion

CT is the modality of choice in the work-up of indeterminate renal mass according to American College of Radiology (ACR) appropriateness criteria [21]. Renal mass characterisation consists of at least 3 phases of acquisition on conventional multidetector CT: unenhanced, corticomedullary and nephrographic phase [22]. In daily clinical practice, a four-phase CT including the excretory phase can be used based on institutional preference [23–27]. However, the more phases of imaging are present, the higher radiation doses the patients are exposed and renal mass characterisation is only based on attenuation which is represented by CT numbers in Hounsfield Units (HU) on conventional single energy CT [24–26]. Recently, DECT has been proved to be useful in showing renal tumor enhancement on iodine density images and renal tumor characterization by showing different iodine contents for different tumor types on nephrographic phase imaging apart from attenuation values [12, 13, 15, 18–20, 25, 28]. Our study has also demonstrated similar findings. Also, our study was the first one to investigate the relationship between benign and malignant tumors. However, mean iodine content of these tumors were quite similar there was no significant difference between these tumors statistically.

The reason why we only obtained nephrographic phase and not corticomedullary phase images on renal mass characterisation DECT protocol was based on the fact that majority of the renal tumors including papillary and chromophobe RCC from malignant tumors, AML and oncocytoma from benign masses reached their enhancement peak in

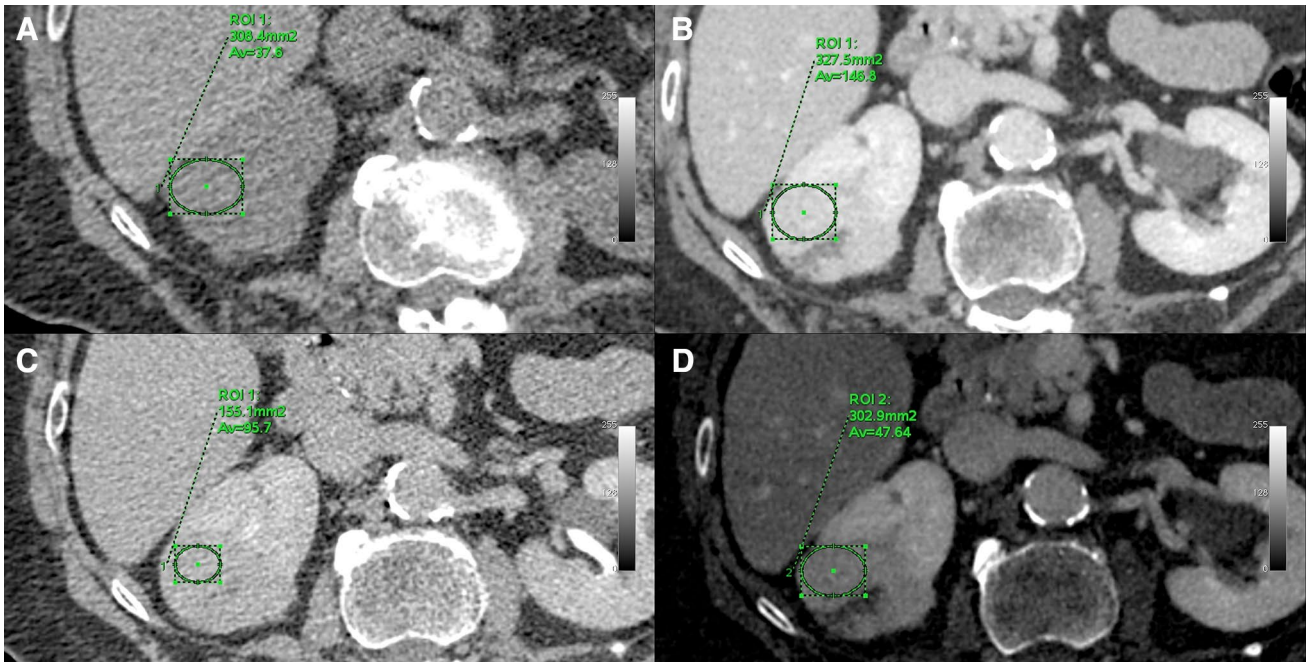

Fig. 1 Axial CT images show an avidly enhancing lesion with washout on true unenhanced image (38 HU) (**a**), nephrographic phase (147 HU) (**b**), excretory phase (96 HU) (**c**) images which is typical of clear cell RCC. Iodine density images (**d**) show marked iodine content inside the lesion (4.76 mg/ml)

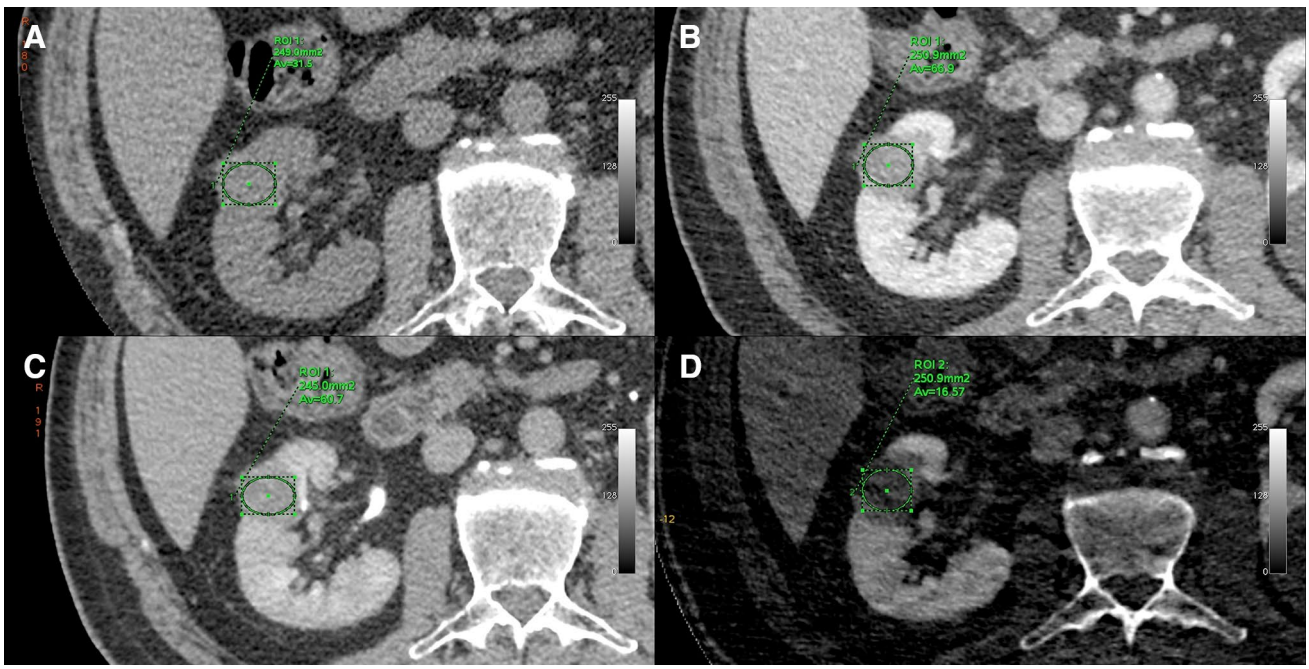

Fig. 2 True unenhanced (31 HU) (**a**), nephrographic phase (67 HU) (**b**), excretory phase (61 HU) (**c**) axial CT images shows a hypovascular papillary RCC with an iodine content of 1.65 mg/ml on iodine density images (**d**)

nephrographic phase. Only clear cell RCC had an enhancement peak in the corticomedullary phase [23]. Therefore, highest attenuation difference between enhanced and unenhanced images and also iodine content in most of renal lesions would be expected in the nephrographic phase. We also showed that there was an excellent-very good positive

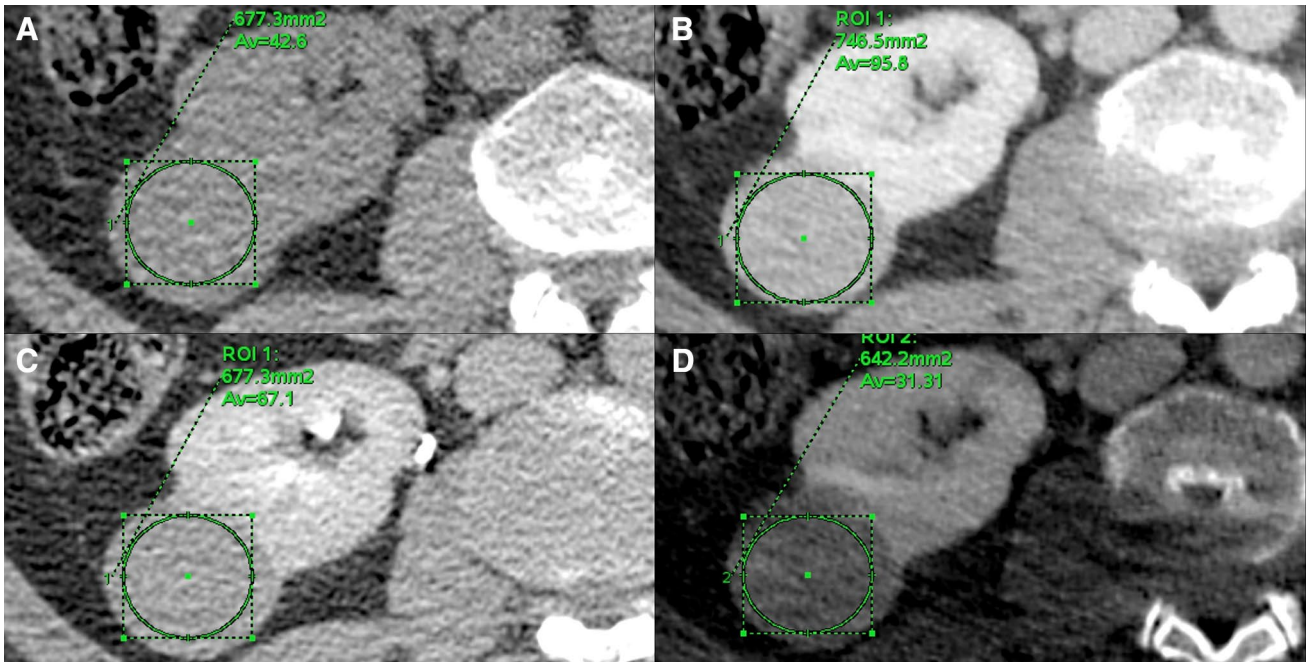

Fig. 3 True unenhanced (42 HU) (**a**), nephrographic phase (96 HU) (**b**), excretory phase (67 HU) (**c**) axial CT images shows a chromophobe RCC with moderate enhancement and an iodine content of 3.13 mg/ml on iodine density images (**d**)

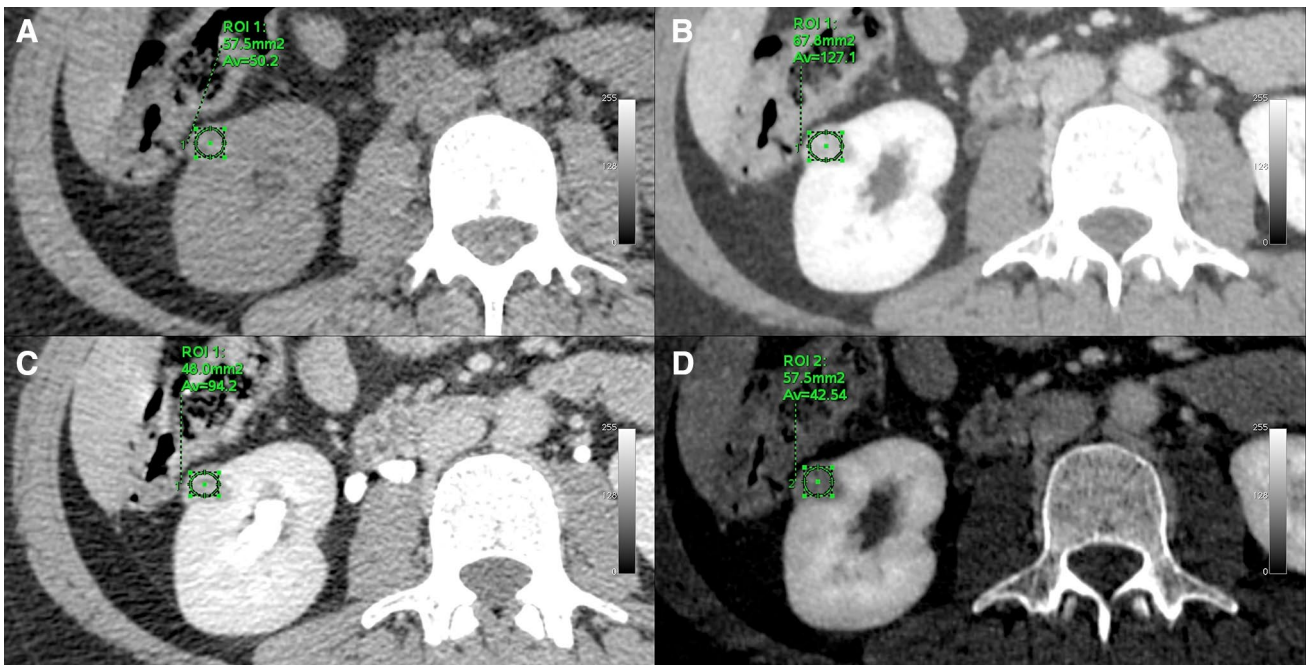

Fig. 4 True unenhanced (50 HU) (**a**), nephrographic phase (127 HU) (**b**), excretory phase (94 HU) (**c**) axial CT images shows a fat-poor AML with marked enhancement and slight washout. Iodine content was calculated as 4.25 mg/ml on iodine density images (**d**)

correlation between absolute contrast enhancement and enhancement ratio with iodine content. Moreover, in the study of Zarzour et al. [20], there were five false-negative papillary RCC and three false-positive complex cysts based on iodine contents in corticomedullary phase. However, there was only one false-positive complex cyst but no

Table 3 Evaluation of iodine content cut-off in nephrographic phase for differentiating clear cell RCC from papillary and non-clear cell RCC

	AUC	Iodine content cut-off (mg/ml)	Sensitivity	Specificity	PPV	NPV	*p*
Clear cell vs. papillary	0.96	2.9	0.91	0.95	0.98	0.79	< 0.001
Clear cell vs. non-clear cell	0.95	3.2	0.89	0.93	0.96	0.81	

AUC area under the curve, *PPV* positive predictive value, *NPV* negative predictive value

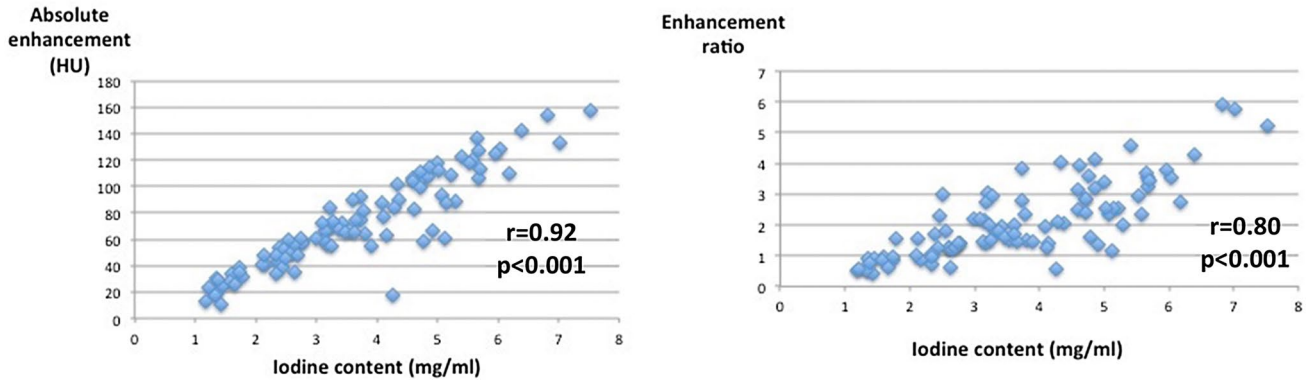

Fig. 5 The scatter plots show the linear correlation with the iodine content and other enhancement parameters

false-negative papillary RCCs were present in the nephrographic phase due to delayed progressive enhancement of papillary RCC. In this study, iodine content threshold for distinguishing clear cell from papillary RCC was 2.71 mg/ml with high accuracy which was close to our threshold of 2.9 mg/ml. In another study [19], this threshold was reported as 0.9 mg/ml but this study was performed on a dual-source DECT platform and their results can not be applied to rsDECT platform.

We also found that papillary and chromophobe RCC could not have been differentiated from each other based on iodine contents and this finding was in line with the single previous study that investigated the same relationship with a different CT platform [18]. Considering that these two types share similar prognosis [2, 3] and their differentiation from each other might not be as crucial as their differentiation from clear cell RCC, we separately classified papillary and chromophobe RCC as non-clear cell RCC and iodine content was significantly different between these groups.

As to the tumor grades, we did not find significant iodine content differences between low-grade and high-grade RCC similar to the majority of the previous studies [18, 20] but Mileto et al. [19] had found significant difference between two groups although there had been a substantial overlap between grade II and III papillary RCC.

The usefulness of virtual unenhanced imaging for replacing true unenhanced images for various abdominal applications including renal mass characterization were previously studied many times on dual-source DECT scanners and good correlation was found between these images in many of these studies [14, 29–31]. However, the number of studies performed with rsDECT is quite low [29] and to our knowledge, ours is the first study to investigate the attenuation difference between true unenhanced and virtual unenhanced images in patients with renal masses. We found significant difference between renal tumor attenuation values on true and virtual unenhanced images. Although the difference between mean attenuation values seemed minimal (38.7 HU vs. 37.2 HU) and attenuation values were well correlated, 8 patients in our study group showed an attenuation difference between 10-14 HU. This kind of difference could lead to erroneous characterization such that a hypovascular papillary RCC could be interpreted as a benign proteinaceous cyst or vice versa. However, imaging parameters such as slice thickness and noise index were not exactly the same and we did not evaluate the image quality of virtual unenhanced images in our cases. Further studies are necessary to enlighten this issue.

The potential of dual-energy CT to reduce radiation dose has also been shown in our study. We could have reduced the DLPs almost by 30% with the use of the unenhanced and nephrographic phase images omitting the excretory phase. Even more could be saved in institutions where four-phase CT including the corticomedullary phase is used. Moreover, we did not observe any significant difference between CTDIvol of single energy excretory phase and dual-energy nephrographic phase although CTDIvol of the single energy unenhanced CT was significantly lower than that of excretory phase. We think that this dose difference could be explained with prospective noise index change that comes with automatic exposure control

and which is inversely proportional with slice thickness increasing CTDIvol with thinner slices.

Major strengths of our study were that it was performed prospectively and in a blinded manner. We could also perform a renal mass characterisation protocol and correlate CT attenuation measurements with iodine content. However, it had some weaknesses. First, sample size was small due to its prospective design and the number of benign lesions were limited.

Secondly, all of the image analyses were done by a single radiologist and interobserver agreement evaluation was not performed against subjective variability and reproducibility of dual-energy iodine quantification. However, Mileto et al. [19] had excellent interobserver agreement in their study and proposed that it may not imperatively necessitate an experienced reader and even inexperienced readers could accurately analyze the images with some training. Also, they proposed that including cystic areas and necrotic parts in a lesion might not have affected iodine content as it is the summed value of enhancing areas in a ROI. On the other hand, in another study [18], ROIs that encompassed the maximum area of enhancement provided more accurate results than largest tumor area or the whole tumor volume encompassing ROIs although the reproducibility was lower. Further research is necessary to elucidate these findings.

Thirdly, we could not propagate the ROIs between true unenhanced and virtual unehanced images automatically and copy the ROIs used in nephrographic phase to the true unehanced images as these images were opened in different reformat viewer modes. So, we might have slightly misplaced the ROIs or adjusted the ROI sizes slightly larger or smaller.

Finally, as different dual-energy platforms provide different thresholds [11], our results could only be applicable to the users of the rsDECT.

In conclusion, despite failing to differentiate between low- and high-grade RCC and benign-malignant tumors, rsDECT contributes to renal tumor characterization by showing higher iodine content in clear cell RCCs compared with non-clear cell RCCs. Moreover, omitting the corticomedullary and excretory phases, radiation dose can substantially be reduced and renal tumors can be characterized in a single nephrographic phase imaging which will be particularly useful in patients with incidental renal tumors on CT performed for nonurinary complaints obviating the need for a dedicated renal protocol CT examination. However, further studies with larger sample size are necessary to validate our findings.

Compliance with ethical standards

Conflict of interest The authors declared no conflicts of interest.

References

1. Frank I, Blute ML, Cheville JC, Lohse CM, Weaver AL, Zincke H (2003) Solid renal tumors: an analysis of pathological features related to tumor size. The Journal of urology 170:2217–2220
2. Amin M, Tamboli P, Javidan J et al (1998) Prognostic impact of histologic subtyping of adult renal epithelial neoplasms (REN)MODERN PATHOLOGY. LIPPINCOTT WILLIAMS & WILKINS 227 EAST WASHINGTON SQ, Philadelphia, PA 19106 USA, pp 75A–75A
3. Cheville JC, Lohse CM, Zincke H, Weaver AL, Blute ML (2003) Comparisons of outcome and prognostic features among histologic subtypes of renal cell carcinoma. The American Journal of Surgical Pathology 27:612–624
4. Bosniak MA (1981) Angiomyolipoma (hamartoma) of the kidney: a preoperative diagnosis is possible in virtually every case. Urologic Radiology 3:135–142
5. Kim KH, Yun BH, Jung SI, et al. (2013) Usefulness of the ice-cream cone pattern in computed tomography for prediction of angiomyolipoma in patients with a small renal mass. Korean Journal of Urology 54:504–509
6. Choudhary S, Rajesh A, Mayer N, Mulcahy K, Haroon A (2009) Renal oncocytoma: CT features cannot reliably distinguish oncocytoma from other renal neoplasms. Clinical Radiology 64:517–522
7. Kim JI, Cho JY, Moon KC, Lee HJ, Kim SH (2009) Segmental enhancement inversion at biphasic multidetector CT: characteristic finding of small renal oncocytoma. Radiology 252:441–448
8. Agrawal MD, Pinho DF, Kulkarni NM, Hahn PF, Guimaraes AR, Sahani DV (2014) Oncologic applications of dual-energy CT in the abdomen. Radiographics 34:589–612
9. Kaza RK, Ananthakrishnan L, Kambadakone A, Platt JF (2017) Update of dual-energy CT applications in the genitourinary tract. American Journal of Roentgenology 208:1–8
10. Marin D, Boll DT, Mileto A, Nelson RC (2014) State of the art: dual-energy CT of the abdomen. Radiology 271:327–342
11. Jacobsen MC, Schellingerhout D, Wood CA, et al. (2017) Intermanufacturer comparison of dual-energy CT iodine quantification and monochromatic attenuation: a phantom study. Radiology 287:224–234
12. Ascenti G, Mazziotti S, Mileto A, et al. (2012) Dual-source dual-energy CT evaluation of complex cystic renal masses. American Journal of Roentgenology 199:1026–1034
13. Graser A, Becker CR, Staehler M, et al. (2010) Single-phase dual-energy CT allows for characterization of renal masses as benign or malignant. Investigative Radiology 45:399–405
14. Graser A, Johnson TR, Hecht EM, et al. (2009) Dual-energy CT in patients suspected of having renal masses: can virtual nonenhanced images replace true nonenhanced images? Radiology 252:433–440
15. Kaza RK, Caoili EM, Cohan RH, Platt JF (2011) Distinguishing enhancing from nonenhancing renal lesions with fast kilovoltage-switching dual-energy CT. American Journal of Roentgenology 197:1375–1381
16. Jung DC, Oh YT, Kim MD, Park M (2012) Usefulness of the virtual monochromatic image in dual-energy spectral CT for decreasing renal cyst pseudoenhancement: a phantom study. American Journal of Roentgenology 199:1316–1319
17. Tappouni R, Kissane J, Sarwani N, Lehman EB (2012) Pseudoenhancement of renal cysts: influence of lesion size, lesion location, slice thickness, and number of MDCT detectors. American Journal of Roentgenology 198:133–137
18. Dai C, Cao Y, Jia Y, et al. (2017) Differentiation of renal cell carcinoma subtypes with different iodine quantification methods

using single-phase contrast-enhanced dual-energy CT: areal vs. volumetric analyses. Abdominal Radiology 43:1–7
19. Mileto A, Marin D, Alfaro-Cordoba M, et al. (2014) Iodine quantification to distinguish clear cell from papillary renal cell carcinoma at dual-energy multidetector CT: a multireader diagnostic performance study. Radiology 273:813–820
20. Zarzour JG, Milner D, Valentin R, et al. (2017) Quantitative iodine content threshold for discrimination of renal cell carcinomas using rapid kV-switching dual-energy CT. Abdominal Radiology 42:727–734
21. Heilbrun ME, Remer EM, Casalino DD, et al. (2015) ACR Appropriateness Criteria indeterminate renal mass. Journal of the American College of Radiology 12:333–341
22. Birnbaum BA, Jacobs JE, Ramchandani P (1996) Multiphasic renal CT: comparison of renal mass enhancement during the corticomedullary and nephrographic phases. Radiology 200:753–758
23. Pierorazio PM, Hyams ES, Tsai S, et al. (2013) Multiphasic enhancement patterns of small renal masses (≤ 4 cm) on preoperative computed tomography: utility for distinguishing subtypes of renal cell carcinoma, angiomyolipoma, and oncocytoma. Urology 81:1265–1272
24. Chandarana H, Rosenkrantz AB, Mussi TC, et al. (2012) Histogram analysis of whole-lesion enhancement in differentiating clear cell from papillary subtype of renal cell cancer. Radiology 265:790–798
25. Neville AM, Gupta RT, Miller CM, Merkle EM, Paulson EK, Boll DT (2011) Detection of renal lesion enhancement with dual-energy multidetector CT. Radiology 259:173–183
26. Young JR, Margolis D, Sauk S, Pantuck AJ, Sayre J, Raman SS (2013) Clear cell renal cell carcinoma: discrimination from other renal cell carcinoma subtypes and oncocytoma at multiphasic multidetector CT. Radiology 267:444–453
27. Zhang J, Lefkowitz RA, Ishill NM, et al. (2007) Solid renal cortical tumors: differentiation with CT. Radiology 244:494–504
28. Mileto A, Marin D, Ramirez-Giraldo JC, et al. (2014) Accuracy of contrast-enhanced dual-energy MDCT for the assessment of iodine uptake in renal lesions. American Journal of Roentgenology 202:W466–W474
29. Borhani AA KM, Iranpour N, Ghodadra A, Sparrow M, Furlan A, Tublin ME (2017) Comparison of true unenhanced and virtual unenhanced (VUE) attenuation values in abdominopelvic single-source rapid kilovoltage-switching spectral CT. Abdominal Radiology (NY) 42:7
30. Ho LM Marin D, Neville AM, Barnhart HX, Gupta RT, Paulson EK, Boll DT (2012) Characterization of adrenal nodules with dual-energy CT: can virtual unenhanced attenuation values replace true unenhanced attenuation values? American Journal of Roentgenology 198:5
31. Lee HA, Lee YH, Yoon KH, Bang DH, Park DE (2016) Comparison of virtual unenhanced images derived from dual-energy CT with true unenhanced images in evaluation of gallstone disease. American Journal of Roentgenology 2016:6